

# Feedback phase sensitivity of a semiconductor laser subject to filtered optical feedback: Experiment and theory

H. Erzgräber\*

*Department of Physics and Astronomy, Vrije Universiteit Amsterdam, De Boelelaan 1081, 1081 HV Amsterdam, The Netherlands*

D. Lenstra

*Faculty for Electrical Engineering, Mathematics, and Computer Science, Technische Universiteit Delft,  
P.O. Box 5031, 2600 GA Delft, The Netherlands*

B. Krauskopf

*Department of Engineering Mathematics, Queen's Building, University of Bristol, Bristol BS8 1TR, United Kingdom*

A. P. A. Fischer

*Laboratoire de Physique des Lasers, Université Paris XIII, UMR CNRS 7538, France*

G. Vemuri

*Indiana University-Purdue University, Indianapolis, Indiana 46202-3273, USA*

(Received 12 April 2007; published 17 August 2007)

We investigate experimentally and theoretically the dynamics of a semiconductor laser subject to filtered optical feedback. Depending on the feedback strength we find dynamical regimes with different dependence on the feedback phase. In particular, the influence of the feedback phase on cw emission and on frequency oscillations is characterized experimentally. We also measure the dependence of the filter mirror distance on the frequency oscillations. In general, good agreement between experiment and theory is found.

DOI: [10.1103/PhysRevE.76.026212](https://doi.org/10.1103/PhysRevE.76.026212)

PACS number(s): 05.45.Xt, 42.65.Sf, 02.30.Ks, 42.55.Px

## I. INTRODUCTION

Stabilizing semiconductor lasers is an important issue since the early days of lasers and many different schemes have been proposed, including conventional optical feedback (COF) from a simple mirror [1,2], phase-conjugate feedback [3–6], or injection from another laser [7]. For example, in Refs. [8,9] COF is used to control the spatiotemporal emission dynamics of a broad-area semiconductor laser.

Here we are concerned with a semiconductor laser subject to filtered optical feedback (FOF), where the feedback light is spectrally filtered before it is re-injected into the laser. Spectral filtering can be achieved, for example, by fiber gratings or optical interferometers; our system is a prototype example of a FOF laser, where the filter is a Fabry-Perot cavity. Indeed the concept of feedback from a resonant cavity is well established [10–15]. However, the effect of the filter on the dynamics of the semiconductor laser was first investigated in [16], where it was shown that filtering the feedback light can suppress low frequency fluctuations. The FOF laser is of interest because it provides the filter frequency (relative to the laser frequency) and the filter width as additional parameters that can be used to influence and control the dynamics of the laser. This makes the FOF laser an attractive choice, for example, for the generation of chaotic laser output for secure communication [17–20] or spectroscopy applications. A further motivation for studying the FOF laser is

the discovery in Ref. [21] that the FOF laser may exhibit frequency oscillations (FOs) on the time scale of the external round trip and with practically constant laser intensity. This is in contrast to the well-known relaxation oscillations (ROs) that involve both the frequency and the intensity of the laser.

In this paper we perform an experimental and theoretical study of the FOF laser, where we concentrate on the coherence aspect of this type of feedback. Specifically, we study how the behavior of the FOF laser depends on the feedback phase, that is, on the phase the laser field accumulates while traveling through the feedback loop. As in any coherent delayed optical feedback scheme, and in contrast to optoelectronic or incoherent feedback, both the amplitude and the phase of the feedback light are important. When the light is traveling through the feedback loop it accumulates the feedback phase  $C_p = \Omega_0 \tau$ , where  $\Omega_0$  is the solitary laser frequency and  $\tau$  is the delay time, that is, the time the light needs to travel through the feedback loop. The feedback phase was identified in Ref. [22] as a key parameter for understanding the high degree of multistability of the FOF laser; see also Ref. [23] and the bifurcation study Ref. [24].

In FOF the feedback phase controls the position of the comb of external filtered modes (EFMs) with respect to the center frequency of the filter. Controlling this phase is essential, e.g., for precision spectroscopy [25]. By contrast, in COF there is no such reference point, and it turns out that the feedback phase is only important for short external cavities [26]; here a short cavity refers to delay times on the order of the period of the laser internal relaxation oscillation frequency. The feedback phase sensitivity for short cavity COF is attributed to the small number of external cavity modes

---

\*Present address: School of Mathematical Sciences, Queen Mary, University of London, London E1 4NS, UK.

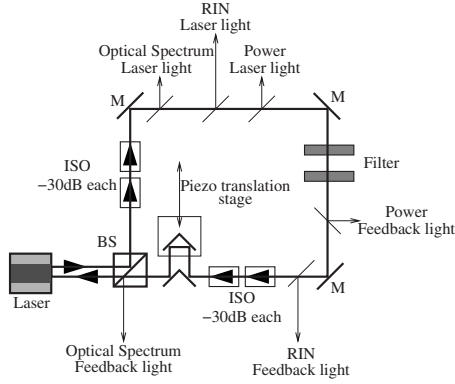


FIG. 1. Setup of the FOF laser with a Fabry-Perot filter, piezotranslation stage, optical isolators (ISO), mirrors (M), and beam splitter (BS). The detection for both the laser field and the feedback field consists of scanning Fabry-Perot interferometers, fast photodiodes, electrical spectrum analyzers, digital oscilloscopes, and slow photodiodes.

[27]. In the FOF laser considered here the delay time is much longer than the period of the relaxation oscillation frequency. Nevertheless, the number of EFM is still small (on the order of 10) because of the use of a narrow filter.

Specifically, we show that for increasing feedback strength the FOF laser may exhibit stable continuous wave (cw) emission, FOs, ROs, quasiperiodic oscillations, and more complicated, possibly chaotic dynamics. Overall, we distinguish seven regimes of the dynamics. For the case of cw emissions and FOs we show in detail how the feedback phase affects the dynamics of the FOF laser. Furthermore, the influence of the filter mirror distance on the period of the FOs is investigated. The experimental measurements are compared with theoretical results of the corresponding rate-equation model to identify the underlying dynamics and bifurcations.

This paper is structured as follows. The experimental setup and the rate equation model is discussed in Sec. II. In Sec. III we present an overview of the different dynamical regimes that are found experimentally when the feedback rate is increased. In Sec. IV we discuss the influence of the feedback phase on the EFM structure. ROs and FOs are introduced in Sec. V. The appearance and disappearance of FOs over one cycle of the feedback phase is shown in Sec. VI. More complicated dynamics for higher feedback rates are discussed in Sec. VII. Finally, in Sec. VIII we discuss the influence of the filter mirror distance on the FOs. We finish with conclusions and an outlook in Sec. IX.

## II. SYSTEM

The FOF laser consists of a semiconductor laser that receives filtered optical feedback as sketched in Fig. 1. We used a commercially available single-mode Fabry-Perot type semiconductor laser emitting at 780 nm with a threshold current of  $I_{th}=43$  mA. Throughout the experiments the laser was operated at a pump current of  $I=70.6$  mA. At this pump current the relaxation oscillation frequency was 3.6 GHz, which has been measured separately. The temperature of the

lasers was stabilized with an accuracy better than 0.01 K. The laser's frequency shift due to changes of the pump current was linear and has been determined as 3.6 GHz/mA. The filter consisted of two flat mirrors with reflectivities  $R=70\%$ , respectively. For the experiments with fixed filter width, the distance between the mirrors was  $D=3.9\pm 0.1$  cm, which is equivalent to a free spectral range of the filter (FSR) of  $3.8\pm 0.1$  GHz. The finesse of the filter has been determined experimentally to be  $f=4\pm 0.5$ , which results in a half filter width at half maximum (HWHM) of  $385\pm 30$  MHz.

At the beam splitter (BS) half of the laser light is directed into the feedback loop, where a total of four optical isolators, with isolation better than  $-30$  dB each, ensure clockwise propagation of the light in the feedback loop. For controlling the feedback phase we use a piezotranslation stage with a mechanical resolution of 20 nm. Given the laser wavelength of 780 nm, this allowed a resolution of 19 measurement points per  $2\pi$  cycle of the feedback phase. The feedback strength was controlled with a combination of a polarizer and a  $\lambda/2$  plate. Without the filter a maximum threshold reduction of about 2 mA (5%) was achieved. Under these conditions the optical spectrum of light emitted by the laser was flat within the 8 GHz bandwidth of the scanning Fabry-Perot interferometers, indicating that the laser was in the coherence collapse regime. With the filter the maximum threshold reduction was about 1 mA (2%). The total length of the feedback loop was  $L=240\pm 1$  cm, which results in a round-trip frequency of the feedback loop of  $125\pm 0.5$  MHz. The detuning between the solitary laser frequency and the center frequency of the filter was about  $400\pm 100$  MHz in the experiment.

The dynamics of the optical field emitted by the laser and the optical field that is fed back into the laser were both detected. For this we used scanning Fabry-Perot interferometers with a free spectral range of 2 and 8 GHz. The respective relative intensity noise (RIN) spectra of the laser light and the feedback light were detected with pigtailed photodiodes and amplifiers with a bandwidth of 250 MHz. Average powers were measured with slow photodiodes.

For the theoretical analysis we use a well-established rate equation model with delay [24,28], which can be written in dimensionless form as

$$\dot{E} = (1 + i\alpha)N(t)E(t) + \kappa F(t), \quad (1)$$

$$T\dot{N} = P - N(t) - [1 + 2N(t)]|E(t)|^2, \quad (2)$$

$$\dot{F} = \Lambda E(t - \tau)e^{-iC_p} + (i\Delta - \Lambda)F(t), \quad (3)$$

where time  $t$  is measured in units of the photon lifetime (10 ps). The variables  $E$  and  $F$  are the complex-valued envelopes of the optical field of the laser and of filtered feedback field, respectively, and  $N$  is the real-valued inversion of the laser. For the self-phase modulation  $\alpha$  and the carrier lifetime  $T$  we use common values for semiconductor lasers. The pump parameter  $P$ , the delay time  $\tau$ , the feedback strength  $\kappa$ , the detuning  $\Delta$ , and the filter width  $\Lambda$  were extracted from the experimental condition. In rescaled units

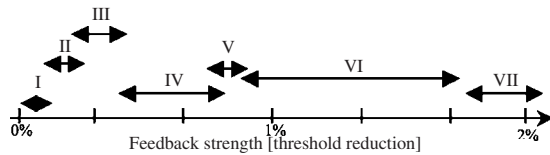


FIG. 2. Overview of the different dynamical regimes I–VII that can be identified for different ranges of feedback strengths (shown here in units of threshold reduction).

(see Ref. [28]) they take the values  $\alpha=5.0$ ,  $T=100$ ,  $P=2.55$ ,  $\tau=743$ ,  $\Delta=-0.014$ ,  $\Lambda=0.014$ .

### III. OVERVIEW OF THE DYNAMICS

To explore the different possible dynamics we took measurements at different feedback levels—from very low feedback to the maximum available feedback level that corresponds to a threshold reduction of about 2%. At each feedback level the feedback phase was increased and decreased to find all possible dynamics. The feedback phase changes by  $2\pi$  when the path in the feedback loop is changed by one wavelength of the laser light. A schematic overview over the different dynamics as a function of feedback strength is shown in Fig. 2, where we distinguish seven regimes I–VII.

In regime I for very low feedback the FOF laser shows continuous wave (cw) emission in discrete frequencies that are determined by the delay in the feedback loop. This introduces a comb of external filtered modes around the center frequency of the filter, where the number of modes is restricted by the bandwidth of the filter. It turns out that all these individual modes are connected: when the feedback phase is changed the FOF laser successively visits all EFMs. As Sec. IV shows, this agrees well with the mathematical analysis of the EFMs. When the feedback strength is increased into regime II the laser shows frequency oscillations (FOs) as the first type of instability. Depending on the value of the feedback phase the FOs increase in amplitude. For higher feedback, in regime III, relaxation oscillations undamp. The ROs may even interact with FOs, which leads to quasiperiodic oscillations. In regime IV more complicated frequency dynamics develops, which in region V does not show any feedback phase dependence. Increasing the feedback strength further into regime VI brings back stable ROs that alternate with complicated frequency dynamics. Finally, in regime VII only ROs can be found; specifically, three different ROs with slightly different frequencies can be found for suitable levels of the feedback phase.

### IV. DEPENDENCE OF THE EXTERNAL FILTERED MODES ON THE FEEDBACK PHASE

As a direct result of the external optical feedback loop, the FOF laser prefers cw operation at certain frequencies. The associated cw states, now known as the external filtered modes or EFMs, can show bistability and multistability. This was demonstrated experimentally, for example, in Ref. [29] where filtered feedback was implemented by an active inter-

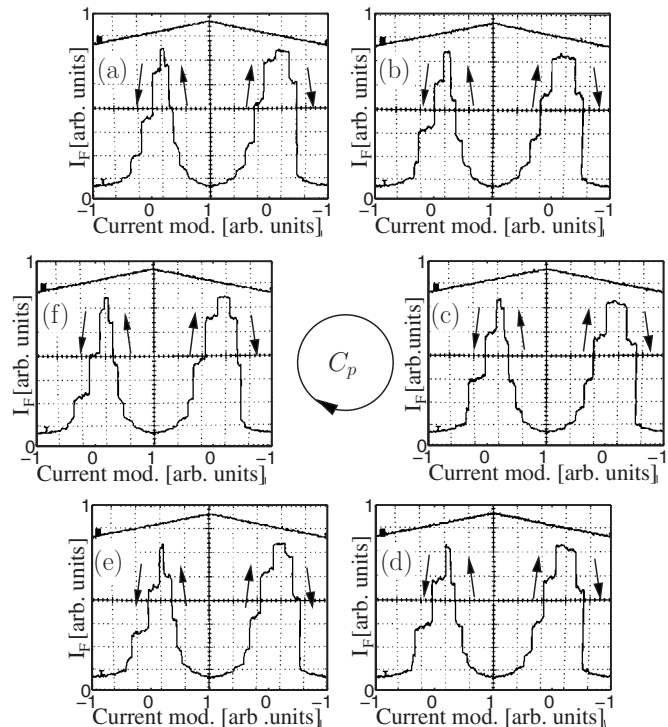


FIG. 3. Measured  $2\pi$  cycle of the EFMs as a function of the detuning. Each panel shows the intensity of the feedback light as a function of increasing and decreasing pump current. The pump current was slowly modulated with a triangular ramp, which is shown in the top of each panel. Arrows indicate the motion of EFM plateaus with the change of the feedback phase. Between consecutive panels the feedback phase  $C_p$  has changed by approximately  $\pi/3$ .

ferometer in combination with electronic feedback. The EFMs for the experimental system considered here were measured in Ref. [23], where the pump current was ramped to vary the laser frequency; hysteresis, bistability, and multistability were reported and it was shown that these effects are described well by a rate-equation model. In this section we consider the influence of the feedback phase on the EFM structure of the system.

Figure 3 shows the experimentally observed evolution of the EFMs over a  $2\pi$  cycle of the feedback phase. Between neighboring panels the length of the feedback loop was increased by approximately  $1/6$  of the laser wavelength, which is equivalent to an increase of the feedback phase by  $\pi/3$ . In each individual panel we visualize the EFMs experimentally by slowly modulating the pump current by a triangular ramp with an amplitude of about 0.5 mA (shown at the top of the panels of Fig. 3) while monitoring the intensity of the feedback field  $I_F$ . The main effect of this small pump modulation is the variation of the laser frequency and therefore of the detuning between the laser and the filter; see also Ref. [23]. Indeed, such small changes of the pump current have a negligible effect on the other parameters.

As the detuning changes, the FOF laser visits successive EFMs. In each panel of Fig. 3 a single EFM corresponds to a plateau with almost constant feedback intensity. Different EFMs have different feedback intensities when following the filter induced intensity profile. Here it is important to realize

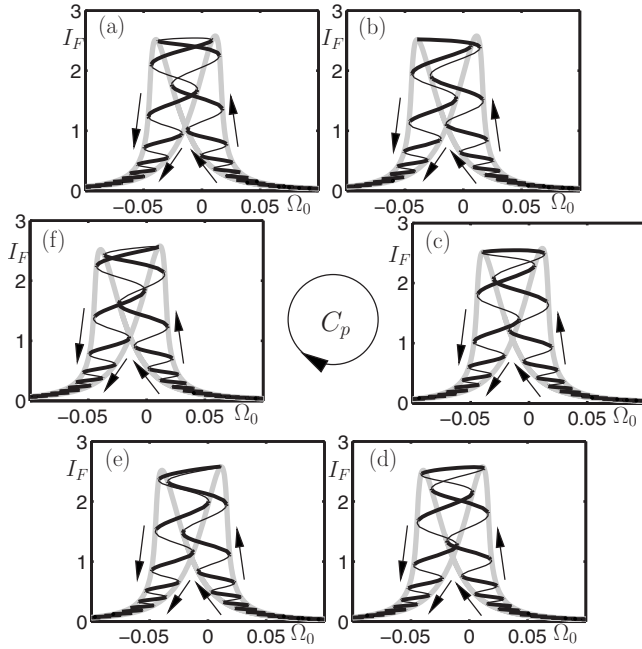


FIG. 4. Computed  $2\pi$  cycle of the EFMs as a function of the detuning for  $\kappa=0.001$ . Each panel shows the intensity of the feedback light  $I_F$  as a function of the solitary laser frequency  $\Omega_0$ . Thick parts of the black EFM curve correspond to stable EFMs. Pairs of stable and unstable EFMs are born in saddle-node bifurcations. The gray curve is the curve of saddle-node bifurcations as parametrized by  $C_p$ . Arrows indicate the motion of EFM plateaus for increasing  $C_p$ . Between consecutive panels the feedback phase  $C_p$  is changed by  $\pi/3$ .

that a different feedback intensity implies a different frequency of the laser light. Thus each plateau indeed corresponds to an EFM with a different frequency. As the feedback phase gradually increases from one panel to the next, the plateaus change their relative position on the underlying filter profile. Their direction of motion is indicated by the arrows in Fig. 3: EFMs on the left flank of the filter continuously move downwards and EFMs on the right flank of the filter move upwards. The transition from panel (a) to (f) and back to (a) involves an increase of the length of the feedback loop by one wavelength and therefore the initial situation is regained. Indeed each plateau has moved to the initial position of its left neighbor and the  $2\pi$  cycle of the feedback phase is closed.

Figure 4 shows the EFMs as computed with the rate-equation model (1)–(3). In each panel the feedback phase  $C_p$  is fixed and the detuning between the laser and the filter is varied by changing the solitary laser frequency  $\Omega_0$ . The resulting EFMs are shown in terms of the feedback intensity  $I_F$ . Note that the EFMs trace out a single closed curve that is bounded by (gray) curves of saddle-node bifurcations. Stable EFMs correspond to the boldface parts of the curve, which form plateaus of a limited  $I_F$  range; indeed in the experiment only these stable EFM branches can be observed. As in the experiment, when the solitary laser frequency  $\Omega_0$  is changed, the feedback intensity  $I_F$  is highest around the filter center frequency  $\Omega_F = -0.014$ . On the individual plateaus  $I_F$  varies only slightly as  $\Omega_0$  is changed. At the end of a plateau the

respective stable EFM disappears in a saddle-node bifurcation and the system jumps to a neighboring stable EFM. The overlap between stable EFM branches is an example of bistability that results in hysteresis effects, meaning that the jumps between plateaus appear for different values for increasing and decreasing detuning  $\Omega_0$ .

## V. RELAXATION AND FREQUENCY OSCILLATIONS

Relaxation and frequency oscillations have different characteristics. The ROs are typical for semiconductor lasers and their frequency (3.6 GHz in our case) depends mainly on solitary laser characteristics such as the pump current of the laser. In the rate equation model (1)–(3) the RO frequency is given by

$$\nu_{RO} = \frac{1}{2\pi} \sqrt{\frac{2P}{T}}. \quad (4)$$

In contrast the frequency of the FOs is determined mainly by the delay time of the external system [21] ( $125 \pm 0.5$  MHz in our case), with a much smaller contribution from the properties of the filter, that is

$$\nu_{FO} \propto \frac{1}{\tau}. \quad (5)$$

More remarkably, for FOs the intensity of the laser light is practically constant, which means that the filter compensates for the high phase-amplitude coupling that is typical for semiconductor lasers; see Ref. [22].

Experimental optical spectra of the laser field, RIN spectra of the laser intensity, and RIN spectra of the feedback intensity for ROs and FOs are shown in Fig. 5. The optical spectrum of ROs [Fig. 5(a1)] shows typical side peaks at the RO frequency  $\nu_{RO}$ . (Note that the optical spectrum is a convolution since the FSR of the scanning Fabry-Perot is 2 GHz but  $\nu_{RO}=3.6$  GHz.) Flat RIN spectra of the laser light [Fig. 5(a2)] and of the feedback light [Fig. 5(a3)] indicate that there are no other dynamics apart from ROs. By contrast, the optical spectrum of FOs [Fig. 5(b1)] exhibits a small shoulder at the right flank of the laser peak. In the RIN spectrum of the feedback light [Fig. 5(b3)] a sharp peak at  $\nu_{FO} = 116.8$  MHz can be seen. It corresponds to the roundtrip frequency in the feedback loop modified by the filter. Higher harmonics in the RIN spectrum indicate a nonharmonic waveform of the oscillation. The flat RIN spectrum of the laser light [Fig. 5(b2)] indicates that the laser intensity is constant.

Figure 6 shows corresponding computed spectra for ROs and FOs as found in Eqs. (1)–(3). In addition we also show time series of the laser intensity  $I_L$  and of the feedback intensity  $I_F$ . ROs can be identified by side peaks in the optical spectrum at  $\pm 3.6$  GHz around the laser peak [Fig. 6(a1)]. Moreover, in the RIN spectrum of the laser light [Fig. 6(a2)] the RO peak at 3.6 GHz can be seen. On the other hand, the RO peak in the RIN spectrum of the feedback light [Fig. 6(a3)] is about 20 dB smaller. Note that the computed RIN spectra show a much wider frequency range; due to bandwidth limitations only the gray-shaded frequency range

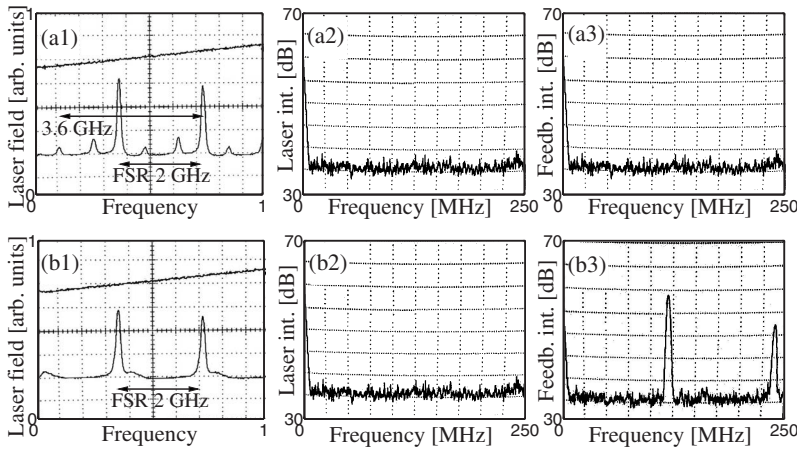


FIG. 5. Measured relaxation and frequency oscillations, namely optical spectrum (a1), RIN spectrum of the laser light (a2), and RIN spectrum of the feedback light (a3) of ROs; and optical spectrum (b1), RIN spectrum of the laser light (b2) and RIN spectrum of the feedback light (b3) of FOs.

could be measured in the experiment; compare with Fig. 5. These characteristics are also brought out in the time series [Fig. 6(a4)], which show a strong oscillation of the laser intensity while the oscillations in the feedback intensity are rather small. By contrast, FOs show a rather different behavior. The optical spectrum [Fig. 6(b1)] shows a comb of equidistant peaks with frequency difference of 123.4 MHz. Note that this frequency difference could not be resolved in the measured spectra. Nevertheless, the structure (of the envelope) agrees well with the experimental spectrum [Fig. 5(b1)], which shows a broadened peak with a steep flank on the low frequency side and a tail on the high frequency side. Moreover, the RIN spectrum of the laser light [Fig. 6(b2)] shows only a small measurable peak, confirming only a weak oscillation in the laser intensity. However, the FO peaks in the RIN spectrum of the feedback light [Fig. 6(b3)] are about

30 dB higher, confirming the strong oscillation of the feedback intensity and hence of the laser frequency. This can also be observed in the time series of the laser intensity and the feedback intensity [Fig. 6(b4)].

### VI. FEEDBACK PHASE SENSITIVITY OF FREQUENCY OSCILLATIONS

Figure 7 shows optical spectra over one  $2\pi$  cycle of the feedback phase. The feedback strength is still low [regime II] and for a certain value of the feedback phase the FOF laser shows cw emission at an EFM. As can be seen in Fig. 7(a), this shows up in the optical spectrum as a single peak at the laser frequency (the second peak is a repetition of this peak

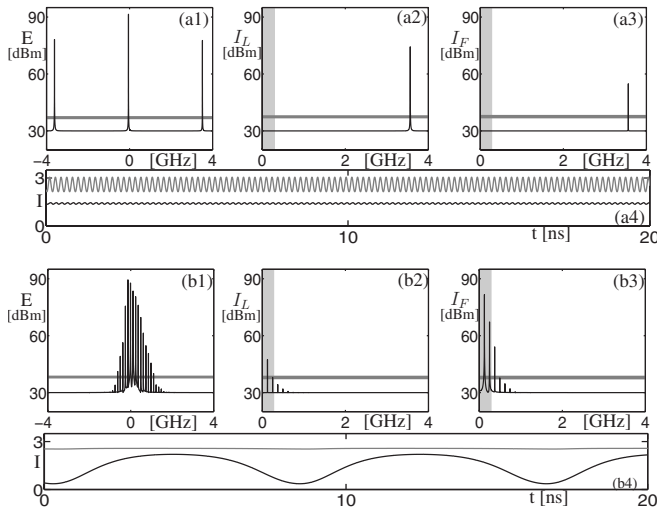


FIG. 6. Computed relaxation and frequency oscillations, namely optical spectrum (a1), RIN spectrum of the laser light (a2), RIN spectrum of the feedback light (a3), and time series (a4) of the laser (gray) and feedback light (black) of ROs; and optical spectrum (b1), RIN spectrum of the laser light (b2), RIN spectrum of the feedback light (b3), and time series (a4) of the laser (gray) and feedback light (black) of FOs. The horizontal gray line indicates the estimated noise level of 10 dB. The light gray region in the RIN spectra is the experimentally accessible frequency range.

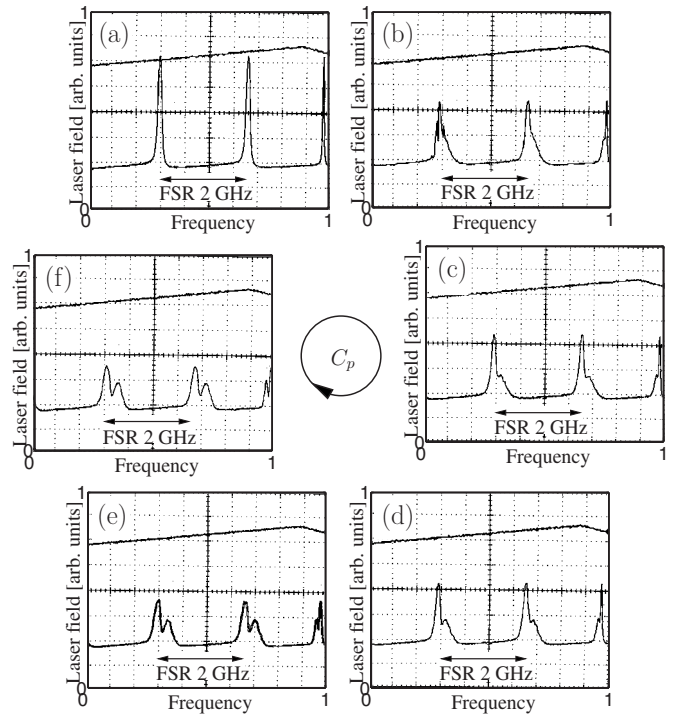


FIG. 7. One cycle of the measured feedback phase dependence in regime I. Shown are optical spectra of the laser field; between consecutive panels the feedback phase has changed by approximately  $\pi/3$ .

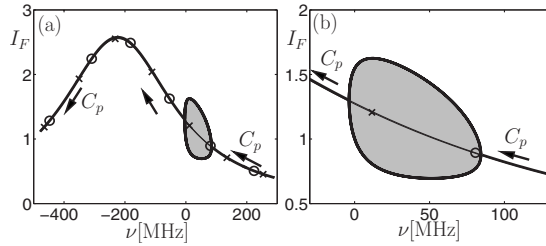


FIG. 8. Computed feedback phase dependence for  $\kappa=0.009$ . The black curve is the feedback intensity of EFMs as parametrized by  $C_p$ ; modes (O) and antimodes (X) for  $C_p=0$  are also shown. The gray bubble (bounded by minimum and the maximum amplitudes) is a region of stable FOs.

due to the limited free spectral range of 2 GHz of the interferometer). As the feedback phase increases, this laser peak broadens [Figs. 7(b) and 7(c)], which indicates that the system approaches a Hopf bifurcation to FOs. This observation is also supported by RIN spectra of the feedback light (not shown here). Eventually, a distinct side peak appears at the right flank of the laser peak [Fig. 7(d)], which then moves further away from the laser peak [Figs. 7(e) and 7(f)]. The side peak disappears quite suddenly when the laser goes back to the EFM at the end of the cycle. Since FOs are modulations of the laser frequency only, the distance between the laser peak and the modulation peak is related to the frequency deviation of the FOs. Thus the cycle of Fig. 7 can be interpreted as the onset of FOs, their gain in amplitude and, finally, a jump back to cw emission of the FOF laser.

Figure 8 illustrates the feedback phase sensitivity and the onset of FOs as computed with the model (1)–(3). Shown is the feedback intensity  $I_F$  as a function of the EFM frequency. Note that this would correspond to the so-called fixed point ellipse in the inversion-frequency representation. The circles (O) and the crosses (X) indicate the location of EFMs, known as modes and antimodes, respectively. These modes trace out the curve in Fig. 8 as  $C_p$  is increased as indicated by the arrows. Indeed the feedback intensity is highest for those EFMs around the filter center, which is approximately at  $-210$  MHz. The gray bubble indicates stable FOs, where the minimum and the maximum amplitude of the feedback intensity of the FOs is plotted. (Recall that oscillations of the feedback intensity imply oscillations of the laser frequency.) As can be seen in the enlarged view of Fig. 8(b), FOs bifurcate from a stable EFM as  $C_p$  is increased, after which the amplitude of the oscillation gradually builds up. Eventually, stable FO disappear again and a quite sudden transition back to a stable EFM can be observed at the left-hand side of the bubble. For this value of  $\kappa$  the width of the stable FO region corresponds approximately to a  $\pi$  range of  $C_p$ . The width of the region of stable FOs may change for different parameter settings. Overall, this theoretical study of the feedback phase sensitivity agrees with the experimental data in Fig. 7.

## VII. MORE COMPLICATED DYNAMICS FOR HIGHER LEVELS OF FEEDBACK

As a first example of dynamics that are more complicated, Fig. 9 shows that also mixed quasiperiodic oscillations with

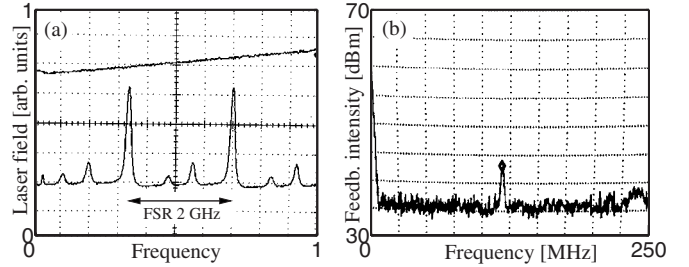


FIG. 9. Optical spectrum (a) and RIN spectrum (b) of the feedback light for quasiperiodic oscillations with RO and FO components.

RO and FO components are possible. This measurement is for a feedback strength from regime III. The optical spectrum shows peaks at the RO frequency, and in addition the RIN spectrum of the feedback light exhibits peaks at the FO frequency. The corresponding RIN spectrum of the laser light is again flat, which indicates that there are no low frequency dynamics in the intensity of the laser light. This type of quasiperiodic oscillation has been predicted by model calculation in Refs. [22,24].

For even higher feedback strength even more complicated or possibly chaotic dynamics can be observed in regimes IV–VI. Again the onset of instabilities manifests itself first in the frequency of the laser.

Figure 10 shows the optical spectrum and a RIN spectrum of the feedback light from regime IV. The optical spectrum shows only peaks at the RO frequency, whereas from the RIN spectrum it can be seen that the dynamics of the laser frequency is now more complicated. The FO peak is broadened, there is a broad peak at a very low frequency of approximately 30 MHz, and there is a broadened peak at a frequency slightly higher than the FO frequency  $\nu_{FO}$ . In addition to these more complicated dynamics, in regime IV, the system may still exhibit pure ROs and mixed quasiperiodic FOs and ROs, depending on the feedback phase. On the other hand, pure FO are no longer found at this level of feedback strength.

For even higher feedback rates in regime V also the optical spectrum indicates complicated dynamics; an example is shown in Fig. 11. Apart from small broadened peaks, which are remnants of the laser peaks, the optical spectrum is now flat. The structure in the RIN spectrum of the feedback field is even more broadened compared to the case depicted in

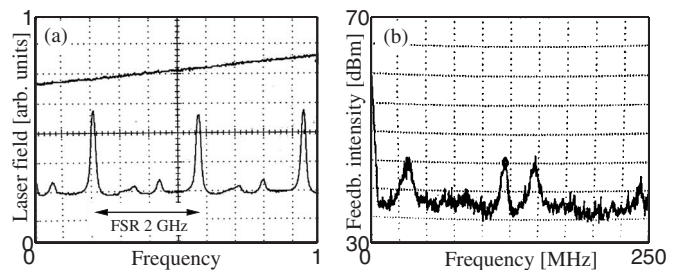


FIG. 10. Optical spectrum (a) and RIN spectrum (b) of the feedback light showing complicated dynamics in the low frequency part of the laser frequency.

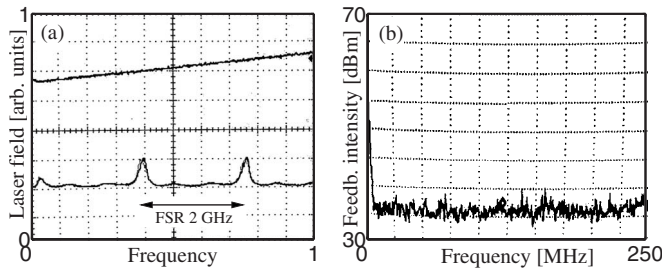


FIG. 11. Optical spectrum (a) and RIN spectrum (b) of the feedback light showing complicated dynamics in both the RO domain and the FO domain.

Fig. 10. Together, this indicates that the FOF laser is in the coherence collapse regime. This interpretation is supported by the fact that no feedback phase sensitivity could be observed (since the latter would rely on the coherence of the laser emission). From the dynamical systems point of view, this might indicate that different attractors for different feedback phases have merged into a larger attractor.

Our measurements indicate that the FOF laser leaves this state of complicated dynamics gradually for increasing feedback strengths. There is the large range of feedback strength, regime VI, where stable ROs appear again; the feedback phase is the control parameter that switches between pure ROs and complicated dynamics as depicted in Fig. 11. In regime VII, that is, for the highest feedback rates that could be realized experimentally, only pure ROs are observed. However, the system was observed to switch between three ROs with slightly different frequencies as the feedback phase is changed. For such high feedback rate more than one transmission line of the Fabry-Perot cavity may contribute to the feedback, which would explain the different ROs observed in this regime.

**VIII. INFLUENCE OF THE FILTER**

So far we have chosen a fixed distance of  $D=3.9 \pm 0.1$  cm between the two mirrors of the Fabry-Perot cavity, which corresponds to a HWHM of the filter of  $385 \pm 30$  MHz. We now vary the distance between these two mirrors and investigate the resulting influence on the observed FOs.

Figure 12 shows how the frequency of the FOs depends on the mirror distance. The laser always operates on the left

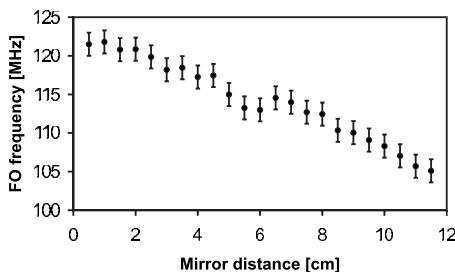


FIG. 12. Measured dependence of the FO frequency on the distance between the filter mirrors; the vertical bars indicate the tuning range of the FO frequency when changing the feedback phase.

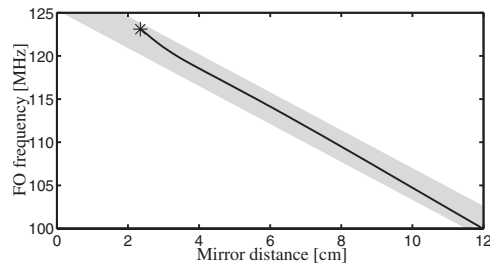


FIG. 13. Computed dependence of the FO frequency on the distance between the filter mirrors. Shown is a (black) curve of FOs; the gray shaded region indicates the possible FO frequencies when  $C_p$  is varied.

flank of the filter profile, and the detuning is about two times the filter HWHM. At each measurement point the value of the FO frequency can be tuned with the feedback phase by about  $\pm 1$  MHz, which is indicated by the vertical bars. The distance between the filter mirrors determines the filter bandwidth. It can be seen that the FO frequency increases as the mirror distance decreases. Namely, the FO frequency depends on the filter bandwidth because the feedback light spends a certain amount of time inside the filter cavity, which comes on top of the actual delay time and hence increases the effective FO period. This filter cavity time is determined by the distance  $L$  between the mirror and the mirror reflectivities. Therefore, as to be expected, in Fig. 12 the FO frequency approaches the value of the roundtrip frequency for very short mirror distances.

Specifically, in a Fabry-Perot cavity the free spectral range (FSR) is determined by the distance  $L$  between the two filter mirrors,  $\Delta_{FSR}=c_0/(2L)$ , where  $c_0$  is the speed of light in vacuum. Furthermore, the finesse is the ratio between the FSR and the full width at half maximum (FWHM) of the individual transmission peaks of the Fabry-Perot cavity. The finesse of the filter cavity was measured in the experiment: over the interval shown in Fig. 12 it is not constant but near an average of 2.5. In fact, the finesse is close to the theoretical limit determined by the reflectivity of the mirror for small distances, and refraction limited for larger distances. Thus in the experiment the contribution of the filter to the FO frequency  $\nu_{FO}$  of Eq. (5) can be estimated as roughly 2.5 times the FSR.

Figure 13 shows the dependence of the FO frequency on the distance between the mirrors of the Fabry-Perot cavity as computed from the rate-equation model (1)–(3); to relate the mirror distance to the filter width  $\Lambda$  we used a constant finesse of 2.5. The gray shaded region indicates the tuning region of the FO frequency for different values of the feedback phase  $C_p$ ; it can be associated with the region delineated by the error bars in Fig. 12. For small mirror distances (which correspond to large filter widths) FOs are born at a supercritical Hopf bifurcation of an EFM; they are stable throughout the shown interval of mirror distances. FOs eventually bifurcate for large mirror distances (small filter widths) in period doubling or torus bifurcations or may end in a homoclinic connection. The exact nature of these bifurcations depends on  $C_p$  and is beyond the scope of this paper.

## IX. CONCLUSIONS AND OUTLOOK

We explored experimentally the dynamics of a semiconductor laser with filtered optical feedback, where we concentrated on the role of the feedback phase. Overall, we could distinguish experimentally seven regimes as a function of the feedback rate, where the FOF laser shows different types of dynamics and different dependence on the feedback phase.

The measurements are in good agreement with computations for the corresponding rate equation model of the FOF laser. Specifically, the measured feedback phase dependence of the observed intensity plateaus under cw emission of the laser was demonstrated to agree with the branches of stable EFMs in the model. We then characterized theoretically and experimentally the frequency and relaxation oscillations. The sequence of measured optical spectra showed how frequency oscillations are created in a Hopf bifurcation as the feedback phase is changed, which has been confirmed with the model equations. Furthermore, we investigated the influence of the filter mirror distance on the frequency of FOs, where we also found good agreement between the experiments and the rate equation model.

For higher feedback rates the dynamics was characterized experimentally by optical spectra of the laser field and RIN spectra of the feedback intensity (corresponding to the laser

frequency). This showed that instabilities in the laser with filtered optical feedback appear in a structured way as the feedback rate increases: first there are instabilities in the frequency of the laser light, and only later are both the frequency and the intensity of the laser affected. We presented two examples of this effect. First, frequency oscillations with constant intensity appear before one finds ROs, for which both the phase and the intensity are oscillating. Second, more complicated dynamics was also found initially in the laser frequency, and only for larger values of the feedback strength also in the laser intensity.

It remains a considerable experimental challenge to map out the possible dynamics in even more detail, for example, in the plane of feedback strength and feedback phase. This would allow one to determine regions where EFMs, FOs, and ROs are stable. Furthermore, transitions to more complicated dynamics could be linked to bifurcation phenomena in the rate equation model. Another interesting issue is to determine the stability ranges of frequency oscillations as a function of the filter detuning and the filter width.

## ACKNOWLEDGMENT

H.E. acknowledges financial support from the promovendfonds of the Vrije Universiteit Amsterdam.

- 
- [1] R. Lang and K. Kobayashi, *IEEE J. Quantum Electron.* **QE-16**, 347 (1980).
  - [2] T. Heil, I. Fischer, and W. Elsässer, *J. Opt. B: Quantum Semi-classical Opt.* **2**, 413 (2000).
  - [3] G. Agrawal and G. Gray, *Phys. Rev. A* **46**, 5890 (1992).
  - [4] G. R. Gray, D. Huang, and G. P. Agrawal, *Phys. Rev. A* **49**, 2096 (1994).
  - [5] P. Kütz and T. Mukai, *Opt. Lett.* **21**, 1369 (1996).
  - [6] K. Green and B. Krauskopf, *Opt. Commun.* **231**, 383 (2004).
  - [7] S. Wiczorek, B. Krauskopf, T. Simpson, and D. Lenstra, *Phys. Rep.* **416**, 1 (2005).
  - [8] S. K. Mandre, I. Fischer, and W. Elsässer, *Opt. Lett.* **28**, 1135 (2003).
  - [9] S. K. Mandre, I. Fischer, and W. Elsässer, *Opt. Commun.* **244**, 355 (2005).
  - [10] R. Drever, J. Hall, F. V. Kowalski, J. Hough, G. Ford, A. Munley, and H. Ward, *Appl. Phys. B: Photophys. Laser Chem.* **31**, 97 (1983).
  - [11] R. Kazarinov and C. Henry, *IEEE J. Quantum Electron.* **QE-23**, 1401 (1987).
  - [12] B. Dahmani, L. Hollberg, and R. Drullingre, *Opt. Lett.* **12**, 876 (1987).
  - [13] H. Li and H. Telle, *IEEE J. Quantum Electron.* **QE-25**, 257 (1989).
  - [14] E. Detoma, B. Tromborg, and I. Montrosset, *IEEE J. Quantum Electron.* **41**, 171 (2005).
  - [15] V. Z. Tronciu, H.-J. Wünsche, M. Wolfrum, and M. Radziunas, *Phys. Rev. E* **73**, 046205 (2006).
  - [16] M. Yousefi and D. Lenstra, *IEEE J. Quantum Electron.* **QE-35**, 970 (1999).
  - [17] G. VanWiggeren and R. Roy, *Science* **279**, 1198 (1998).
  - [18] I. Fischer, Y. Liu, and P. Davis, *Phys. Rev. A* **62**, 011801(R) (2002).
  - [19] A. Argyris, D. Syvridis, L. Larger, V. Annovazzi-Lodi, P. Colet, I. Fischer, J. García-Ojalvo, C. R. Mirasso, L. Pesquera, and K. A. Shore, *Nature (London)* **438**, 343 (2005).
  - [20] A. Uchida, F. Rogister, J. García-Ojalvo, and R. Roy, *Prog. Opt.* **48**, 203 (2005).
  - [21] A. P. A. Fischer, M. Yousefi, D. Lenstra, M. W. Carter, and G. Vemuri, *Phys. Rev. Lett.* **92**, 023901 (2004).
  - [22] H. Erzgräber, B. Krauskopf, D. Lenstra, A. Fischer, and G. Vemuri, *Phys. Rev. E* **73**, 055201(R) (2006).
  - [23] A. Fischer, O. Andersen, M. Yousefi, S. Stolte, and D. Lenstra, *IEEE J. Quantum Electron.* **36**, 375 (2000).
  - [24] H. Erzgräber, B. Krauskopf, and D. Lenstra, *SIAM J. Appl. Dyn. Syst.* **6**, 1 (2007).
  - [25] J. Labaziewicz, P. Richerme, K. Brown, I. Chuang, and K. Hayasaka, *Opt. Lett.* **32**, 572 (2007).
  - [26] A. Tabaka, K. Panajotov, I. Veretennicoff, and M. Sciamanna, *Phys. Rev. E* **70**, 036211 (2004).
  - [27] T. Heil, A. Uchida, P. Davis, and T. Aida, *Phys. Rev. A* **68**, 033811 (2003).
  - [28] K. Green and B. Krauskopf, *Opt. Commun.* **258**, 243 (2006).
  - [29] J. Ohtsubo and Y. Liu, *Opt. Lett.* **15**, 731 (1990).